Generation of Extreme Wave Composed of Ring Waves in a Circular Basin

Munehiko Minoura, Ryo Takahashi
Department of Naval Architecture and Ocean Engineering, Osaka University
Osaka, Japan

Etsuro Okuyama
Akishima Laboratory (Mitsui Zosen) Inc.
Tokyo, Japan

Shigeru Naito
Department of Naval Architecture and Ocean Engineering, Osaka University
Osaka, Japan

ABSTRACT

Arbitrary wave field is well-known to be represented by superposing of Bessel functions with the Fourier-Bessel series expansion. According to the addition theorem, the Bessel function of which origin is put on the center of a circle is described by superposing of Hankel functions of which origins are put on the circumference of a circle. Using this relation between these functions, the present paper proposes the methods on generating extreme waves by superposing of ring waves expressed by the Hankel function. As a result of simulation and experiment in the circular wave basin, which is called *AMOEBA*, the validity of the proposed method is clarified.

KEY WORDS: *AMOEBA*; element absorbing wave-maker; addition theorem; Fourier-Bessel expansion; extreme wave

INTRODUCTION

Ship behavior in extreme wave has not been sufficiently clarified. The characteristics of ship responses in extreme wave are often obtained from model experiments in a towing tank or a wave basin. The extreme wave with big height and steepness is usually generated by focusing element regular waves at a specific location with the same phase. This extreme wave appears in an instant because of wave divergence.

The theory of extreme-wave generation is based on the superposition of long-crested waves propagating forward. The long-crested waves is usually generated by the snake motion of element (segmented) wave-makers put on a rectangular basin (Madsen 1974, Ishida *et al.* 1984, Takezawa *et al.* 1992). However, a wave generated by an element wave-maker is a ring wave. Hence it

is better that the theory of extreme-wave generation is based on the superposition of ring waves. This paper proposes a mathematical method of generation of extreme waves by ring waves. Consequently we expect to generate more arbitrary and accurate wave field.

Ring wave is expressed by the Bessel function mathematically. It disperses outward from a source in the forward time and focuses at the source point in the reverse time. To generate ring wave, we require a wave basin furnishing many element absorbing wave-
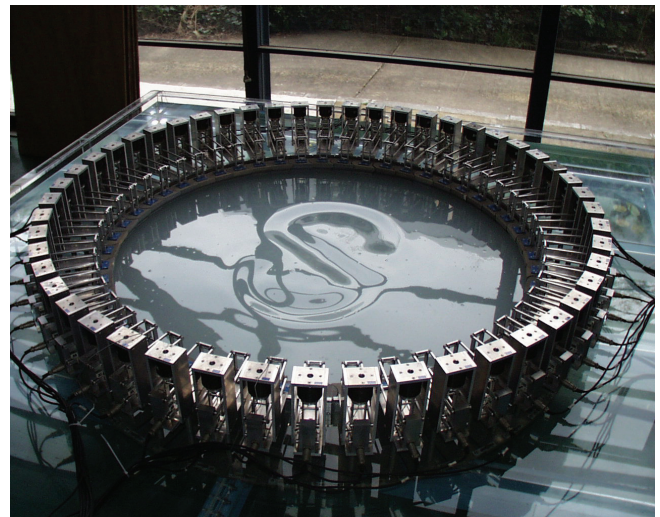

Fig. 1 Photograph of *AMOEBA.*

makers around the whole of the basin. Authors (Naito *et al.* 1999) have developed this basin of which name is *AMOEBA*; *Advanced Multiple Organized Elemental BAsin* consisting of fifty units of element absorbing wave-makers as shown in Fig. 1. This photograph shows a letter S appearing on the water surface in the *AMOEBA*. This letter is written by many focused wave on the path of the letter. However, the wave height and steepness are uncertain. The wave height an steepness of the designed wave focusing at a specific location must be certain. For this aim, the relation between the designed wave and ring waves generated by element wave-maker must be clarified.

To validate this mathematical expansion, using ring waves we generate the extreme wave on the free surface in the basin in an instant. Wave height measured with a wave probe also agrees to the target height of the designed extreme wave. These results conclude the proposed method is valid for generating the extreme wave.

WAVES EXPRESSED BY BESSEL FUNCTION

Waves diverging from a periodical wave source put on a water surface is expressed by $H_0^{(1)}$;the 0th order Hankel function of the first kind given by a first order solution of the Laplace's equation. Naito *et al.*(1994, 1998, 2006) have expressed this wave source by an element wave-maker. Furthermore, they have proposed an element absorbing wave-maker which can generate divergent waves and absorb incident waves at the same time. This wave absorption is based on the theory by Miligram(1970), Falnes(1978), Bessho(1980) and Salter(1981). The *AMOEBA* developed by Naito *et al.*(1999) has these element absorbing wave-maker. It is confirmed by experiments that the reflected waves on the wave-maker does not stand in the *AMOEBA*. According to the linear theory, an arbitrary wave field is described by the superposition of waves generated by element absorbing wave-makers.

A polar coordinate system is defined on a water surface and the points P and Q are defined as Fig. 2. The point Q is located inside the circle with the center at the origin and the radius r_0, the length of OP. An element absorbing wave-maker is put at the point P. Arguments of P and Q are represented as ϕ and θ respectively. Each position vector is defined as

$$\vec{OP} = \mathbf{r}_0, \quad \vec{OQ} = \mathbf{r}, \quad \vec{PQ} = \mathbf{s}. \tag{1}$$

The following relationship is obtained.

$$\mathbf{s} = \mathbf{r} - \mathbf{r}_0. \tag{2}$$

Let r, s denote the magnitudes of the vectors $\mathbf{r}, \mathbf{s}$ respectively. The distance between P and Q is indicated by s:

$$s = \sqrt{\mathbf{s} \cdot \mathbf{s}} = \sqrt{r^2 + r_0{}^2 - 2rr_0 \cos(\theta - \phi)}. \tag{3}$$

Then wave elevation at the point Q is described as

$$\zeta(\mathbf{r}, t) = \Re\left[H_0^{(1)}[ks] e^{-i\omega t}\right], \tag{4}$$

where k is a wave number and ω an angular frequency. These numbers satisfy the divergence relation $\omega^2 = kg \tanh kh$. The notations h and g are water depth and gravity acceleration respectively. According to the addition theorem of the Hankel function, in $r < r_0$ we obtain

$$H_0^{(1)}[ks] = \sum_{m=-\infty}^{\infty} J_m[kr] H_m^{(1)}[kr_0] e^{im(\theta - \phi)}, \tag{5}$$
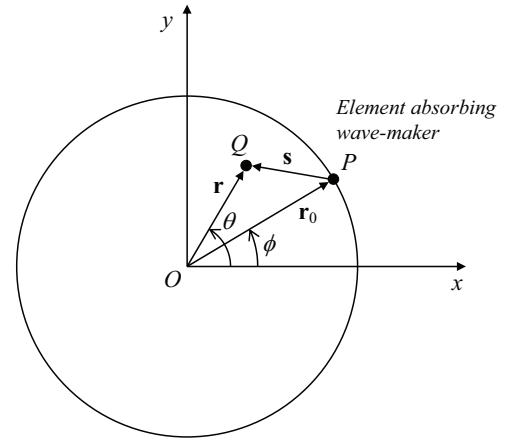

Fig. 2 Coordinate system.

where J_m is the m-th order Bessel function of the first kind. Multiplying $e^{in\phi}$ in the both sides of this equation and integrating for ϕ from 0 to 2π, we can take only the n-th order term in the right-hand side. Consequently the Bessel function of the first kind is expressed by

$$J_n[kr] e^{in\theta} = \frac{1}{2\pi H_n^{(1)}[kr_0]} \int_0^{2\pi} H_0^{(1)}[ks] e^{in\phi} d\phi. \tag{6}$$

This equation implies that the Bessel function expresses the wave field generated by the element absorbing wave-makers put on the circumference of the radius r_0 without gaps between wave-makers. The function $e^{in\phi}$ represents the phase difference between wave-makers. When $n = 0$, this phase difference disappears and perfect ring waves appear. The wave field generated by real wave-makers can be approximated by the discrete equation of Eq. 6:

$$J_n[kr] e^{in\theta} \sim \frac{\Delta\phi}{2\pi H_n^{(1)}[kr_0]} \sum_{j=1}^{N} H_0^{(1)}[ks_j] e^{in\phi_j}, \tag{7}$$

where N denotes the number of wave-makers.

WAVE GENERATING FORCE OF WAVE-MAKER

An arbitrary wave field, except for breaking waves, is geometrically described by the trigonometric series expansion for an angular coordinate denoted by θ and the Fourier-Bessel series expansion for a radial coordinate denoted by r. Let $\zeta(r, \theta)$ denote the arbitrary wave elevation at the time $t = 0$. This elevation is described as

$$\zeta_a(r, \theta) = \sum_{n=0}^{\infty} \sum_{m=1}^{\infty} (A_{nm} \cos n\theta + B_{nm} \sin n\theta) J_n[k_{nm}r], \tag{8}$$

where k_{nm} indicates the wave number for the radial coordinate. Complex number usually makes wave problems simpler and is given as

$$\zeta_a(r, \theta) = \sum_{n=-\infty}^{\infty} \sum_{m=1}^{\infty} C_{nm} e^{in\theta} J_n[k_{nm}r], \tag{9}$$

where,

$$C_{nm} = \begin{cases} \dfrac{1}{2}\left(A_{nm} - iB_{nm}\right) & \text{for} \quad n > 0 \\[2mm] A_{0m} & \text{for} \quad n = 0 \\[2mm] \dfrac{(-1)^n}{2}\left(A_{nm} + iB_{nm}\right) & \text{for} \quad n < 0 \end{cases} \quad (10)$$

$$A_{nm} = A_{-nm}, \quad B_{nm} = B_{-nm},$$
$$k_{nm} = k_{-nm} > 0.$$

The wave elevation at the time t is expressed by the real part of the complex wave field given by the product of Eq. 9 and the time oscillating component as

$$\zeta(r,\theta,t) = \Re\left[\sum_{n=-\infty}^{\infty}\sum_{m=1}^{\infty} C_{nm}e^{in\theta}J_n\left[k_{nm}r\right]e^{-i\omega_{nm}t}\right], \quad (11)$$

where $\omega_{nm} = \omega_{-nm} > 0$. Substituting Eq. 7 into Eq. 11 gives

$$\zeta(r,\theta,t) =$$
$$\Re\left[\sum_{j=1}^{N}\sum_{n=-\infty}^{\infty}\sum_{m=1}^{\infty}\frac{C_{nm}\Delta\phi e^{in\phi_j}}{2\pi H_n^{(1)}[k_{nm}r_0]}H_0^{(1)}[k_{nm}s_j]e^{-i\omega_{nm}t}\right]. \quad (12)$$

Eq. 4 describes a wave field generated by the element absorbing wave-maker located at the point P. The component $e^{-i\omega t}$ in Eq. 4 expresses the oscillation of this wave-maker. Therefore applying the transfer function for $e^{-i\omega t}$, we obtain the wave generating force of this wave-maker. Naturally the component in Eq. 12:

$$\sum_{n=-\infty}^{\infty}\sum_{m=1}^{\infty}\frac{C_{nm}\Delta\phi e^{in\phi_j}}{2\pi H_n^{(1)}[k_{nm}r_0]}e^{-i\omega_{nm}t}$$

represents the oscillation of the element absorbing wave-maker located at the point P_j. Applying the transfer function for this component provides the wave generating force of this wave-maker. The transfer function represented by complex number is defined as $F(\omega_{nm})$. Then the wave generating force $z_j(t)$ of this wave-maker is given by

$$z_j(t) = \Re\left[\sum_{n=-\infty}^{\infty}\sum_{m=1}^{\infty}F(\omega_{nm})\frac{C_{nm}\Delta\phi e^{in\phi_j}}{2\pi H_n^{(1)}[k_{nm}r_0]}e^{-i\omega_{nm}t}\right]. \quad (13)$$

DINI EXPANSION OF WAVE FIELD

The wave number k_{nm} is determined from the boundary condition at the basin wall where element absorbing wave-makers are installed. The boundary condition is concerned with the orthogonality of the Bessel function. Getting back to the Bessel's differential equation, we obtain the integral equation of the Bessel function as follows:

$$\left(k_i^2 - k_j^2\right)\int_0^{r_0} rJ_n\left[k_ir\right]J_n\left[k_jr\right]dr =$$
$$r_0\left(J_n\left[k_ir_0\right]\frac{dJ_n\left[k_jr\right]}{dr}\bigg|_{r=r_0} - J_n\left[k_jr_0\right]\frac{dJ_n\left[k_ir\right]}{dr}\bigg|_{r=r_0}\right). \quad (14)$$

When the right-hand side of this equation equals to zero for $k_i \neq k_j$, the orthogonality of the Bessel function is satisfied. The simplest condition due to the orthogonality is a couple of
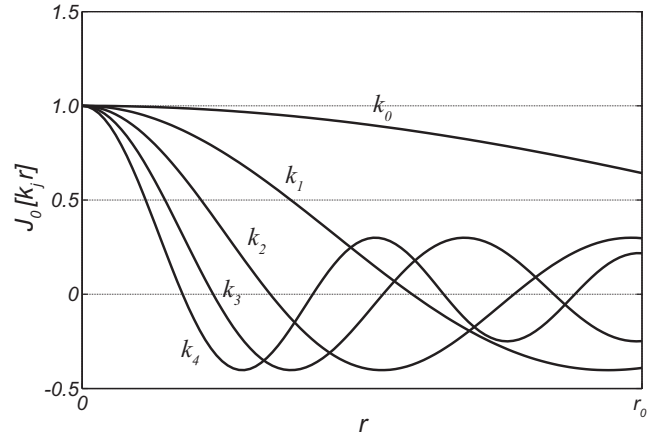

Fig. 3 Profile of the Bessel function satisfying the orthogonarity with respect to r_0 based on the Dini expansion.

$J_n\left[k_ir_0\right] = 0$ and $J_n\left[k_jr_0\right] = 0$. However, this condition makes the plentifulness of wave field reduced because the wave elevation at the boundary must be restricted to zero. $J_n\left[k_jr_0\right] = 0$ implies $\zeta_a(r_0,\theta) = 0$.

Another condition deriving the orthogonality is

$$k_jJ_n'\left[k_jr_0\right] + p_nJ_n\left[k_jr_0\right] = 0. \quad (15)$$

The prime symbol denotes the derivative. The parameter p_n is defined as

$$p_n = -k_i\frac{J_n'\left[k_ir_0\right]}{J_n\left[k_ir_0\right]}. \quad (16)$$

This parameter p_n is usually fixed to an arbitrary constant value. This condition is available for more various wave fields because the wave elevation at the basin wall is not restricted to zero. The profile of the Bessel function for some wave numbers satisfying this orthogonality is shown in Fig. 3. The Fourier-Bessel series expansion in the condition of Eq. 15 is known as the Dini expansion. Using the series of wave number k_j obtained from this equation, we can express the orthogonality by

$$\int_0^{r_0} rJ_n[k_jr]J_n[k_\ell r]dr$$
$$= \begin{cases} 0 & \text{for} \quad j \neq \ell, \\[2mm] \dfrac{(p_nr_0)^2 + (k_jr_0)^2 - n^2}{2k_j^2}J_n[k_jr_0]^2 & \text{for} \quad j = \ell. \end{cases} \quad (17)$$

According to this orthogonality, multiplying $rJ_n[k_{n\ell}r]$ in both sides of Eq. 9 and integrating for ϕ from 0 to 2π and for r from 0 to r_0, we obtain the coefficient C_{nm} by

$$C_{nm} = \frac{u_{nm}^2}{\pi\left(p_n^2r_0^2 + u_{nm}^2 - n^2\right)J_n\left[u_{nm}\right]^2} \times$$
$$\int_0^1\int_0^{2\pi}\zeta_a(r_0\xi,\theta)\xi J_n\left[u_{nm}\xi\right]e^{-in\theta}d\theta d\xi, \quad (18)$$

where $u_{nm} = k_{nm}r_0$. The integral range for the radial coordinate is normalized. Although $\zeta_a(r,\theta)$ represented by Eq. 9 is given as a real number, C_{nm} can be determined from $\zeta_a(r,\theta)$ given as a complex number.
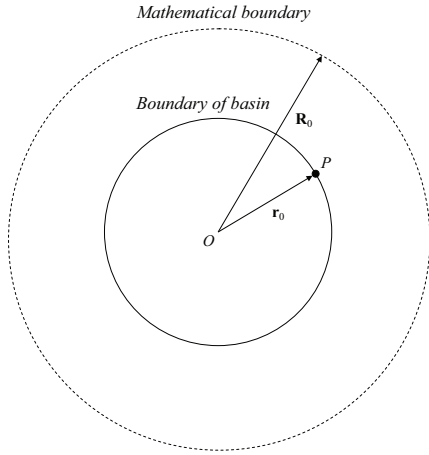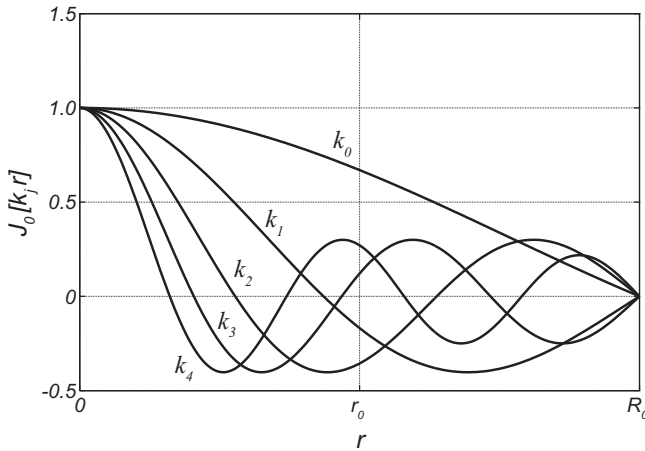
Fig. 4 Mathematical boundary.

Fig. 5 Profile of the Bessel function satisfying the orthogonality with respect to R_0. The mathematical boundary is indicated by R_0 and the basin boundary by r_0.

FOURIER-BESSEL EXPANSION OF WAVE FIELD

The boundary satisfying the orthogonality is mathematically permitted to exist outside the circular basin. We define the radius R_0 which is larger than the basin radius r_0 as shown in Fig. 4. The simplest boundary condition for the orthogonality is expressed by

$$J_n[k_j R_0] = 0. \qquad (19)$$

Using the series of wave number k_j obtained from this equation, we can express the orthogonality by

$$\int_0^{R_0} r J_n[k_j r] J_n[k_\ell r] dr = \begin{cases} 0 & \text{for } j \neq \ell, \\ \dfrac{R_0{}^2}{2} J_{n+1}[k_j R_0]^2 & \text{for } j = \ell. \end{cases} \qquad (20)$$

Then the restriction of the plentifulness of wave field is removed because $J_n[k_j r_0] = 0$ restricting wave elevation to zero at the basin wall is not required like the Dini expansion. The profile of the Bessel function satisfying this orthogonality is shown in Fig. 5. According to Eq. 20, multiplying $r J_n[k_{n\ell} r]$ in both sides of
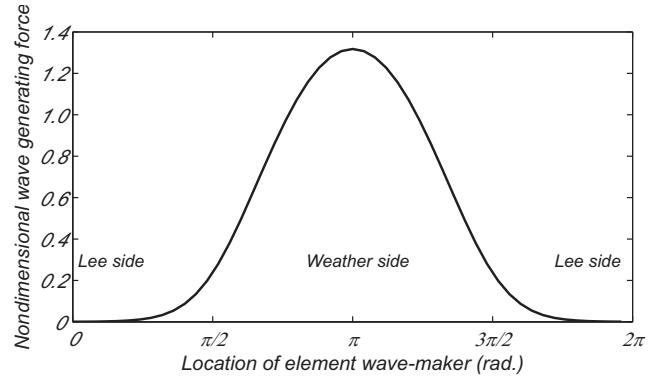

Fig. 6 Wave generating force of element absorbing wave-maker put on the circumference of the basin.
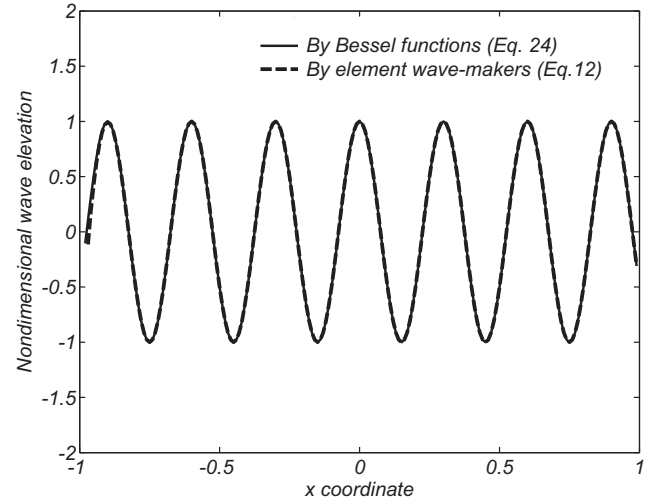

Fig. 7 Wave elevation on the x-coordinate at $t = 0$.

Eq. 9 and integrating for ϕ from 0 to 2π and for r from 0 to R_0, we obtain the coefficient C_{nm} by

$$C_{nm} = \frac{1}{\pi J_{n+1}[v_{nm}]^2} \int_0^1 \int_0^{2\pi} \zeta_a(R_0\xi, \theta) \xi J_n[v_{nm}\xi] e^{-in\theta} d\theta d\xi, \qquad (21)$$

where $v_{nm} = k_{nm} R_0$. Eq. 19 implies that the enlargement of the radius R_0 makes the fundamental wave number k_0 small. Hence the large R_0 gives the higher resolution of wave expansion.

VERIFICATION BY LONG-CRESTED REGULAR WAVE

The complex wave amplitude of the long-crested regular wave with the wave number k traveling to the positive direction of x-coordinate is expressed by

$$\zeta_a(r, \theta) = \exp(ikx) = \exp(ikr\cos\theta). \qquad (22)$$

When this equation is substituted into Eq. 21, R_0 is eliminated and C_{nm} is obtained by

$$C_{nm} = i^n. \qquad (23)$$

In the derivation of this equation the integral description of the Bessel function(Abramowitz *et al.* 1972) are applied. Substi-
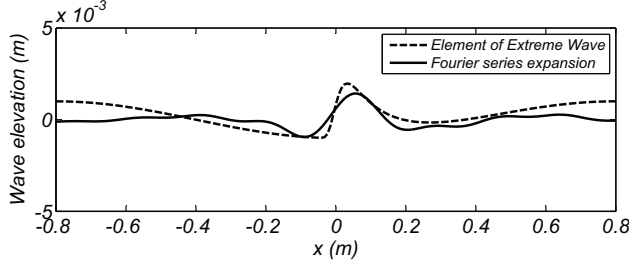
Fig. 8 Snapshot of extreme wave at $t = 0$.
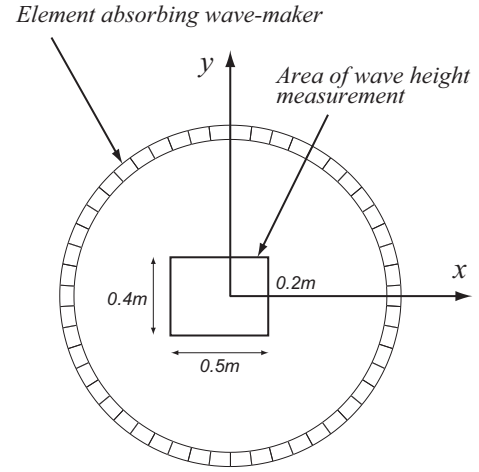

Fig. 9 Element component of extreme wave on the x-coordinate at $t = 0$.

Fig. 10 Area of wave height measurement. Wave height is measured at 546 points with 2cm mesh interval in this area.

tuting Eq. 23 into Eq. 11 consequently gives the well-known equation describing the long-crested regular wave:

$$\zeta(r, \theta, t) = \Re \left[\sum_{n=-\infty}^{\infty} i^n e^{in\theta} J_n [kr] e^{-i\omega t} \right]. \quad (24)$$

Substituting Eq. 23 into Eq. 13 provides the wave egeneration force of each wave-maker:

$$z_j(t) = \Re \left[\sum_{n=-\infty}^{\infty} F(\omega) \frac{i^n \Delta\phi e^{in\phi_j}}{2\pi H_n^{(1)} [kr_0]} e^{-i\omega t} \right]. \quad (25)$$

Fig. 6 shows amplitude values of $z_j(t)$ for $N = 50$, $\Delta\phi = 2\pi/N$, $r_0 = 1.0$ and $k = 2\pi/0.3$. The weather side is at $\phi_j = \pi$ and the lee side is at $\phi_j = 0$. In the weather side wave-makers obviously generate waves. Fig. 7 shows wave elevations presented by the Bessel functions and generated by the element absorbing wave-makers in the section on the x-coordinate at $t = 0$. The wave elevation by the Bessel functions is expressed by Eq. 24 and the wave elevation by the element absorbing wave-makers is expressed by Eq. 12. Both wave elevations completely agree. Eq. 12 is consequently verified.

DESIGNING OF EXTREME WAVE

Authors define the extreme wave as the wave having big height and big steepness. In this paper the extreme wave is provided by

$$\zeta_a(r, \theta) = \int_{-\pi}^{\pi} \left[a_0 \exp \left\{ -a_2 r \cos(\theta - \varphi) - e^{-a_3 r \cos(\theta - \varphi)} \right\} \right.$$
$$\left. -0.2a_0 \cos \left\{ \frac{\pi}{r_0} r \cos(\theta - \varphi) \right\} \right] d\varphi, \quad (26)$$

which describes the wave elevation at the time $t = 0$. For practical calculations, we deal the discrete formula described as

$$\zeta_a(r, \theta) = \sum_{\mu=-M}^{M} \left[a_1 \exp \left\{ -a_2 r \cos(\theta - \varphi_\mu) - e^{-a_3 r \cos(\theta - \varphi_\mu)} \right\} \right.$$
$$\left. -0.2a_1 \cos \left\{ \frac{\pi}{r_0} r \cos(\theta - \varphi) \right\} \right], (27)$$

where $\varphi_\mu = \mu\varphi_0$ and $\varphi_0 = \pi/M$. This extreme wave is shown in Fig. 8 for $a_1 = 0.005$, $a_2 = 10$, $a_3 = 50$ and $M = 12$. The element wave progressing from $\varphi_j = 0$ is described by

$$\zeta_0(x) = a_1 \exp \left(-a_2 x - e^{-a_3 x} \right) - 0.2a_1 \cos \left(\frac{\pi}{r_0} x \right), \quad (28)$$

where $x = r \cos \theta$. This describes a long-crested wave. Its profile is shown by the broken line in Fig. 9. The extreme wave $\zeta_a(r, \theta)$ is obtained by the superposition of element waves progressing from the range of $-\pi$ to π. The element wave $\zeta_0(x)$ is assumed to progress to the negative direction of the x-coordinate. To take account into the dispersion relation of wave, we apply the Fourier series expansion for $\zeta_0(x)$.

$$\hat{\zeta}_0(x) = \sum_{\nu=-\infty}^{\infty} D_\nu \exp \left(-i\kappa_\nu x \right), \quad (29)$$

where,

$$D_\nu = \frac{1}{2L} \int_{-L}^{L} \zeta_0(x) \exp \left(i\kappa_\nu x \right) dx,$$

$$\kappa_\nu = \nu \frac{2\pi}{L}.$$

The wave profile described by Eq. 29 is shown by the solid line in Fig. 9. The wave numbers are restricted within $\kappa_\nu = 10$ to 33 due to the capability of the element absorbing wave-maker of the *AMOEBA*. Although this wave profile does not agree with the wave profile by Eq. 28, the characteristics of extreme wave are inherent. Therefore we use the wave described by Eq. 29 as the designed extreme wave with the wave dispersion relation.
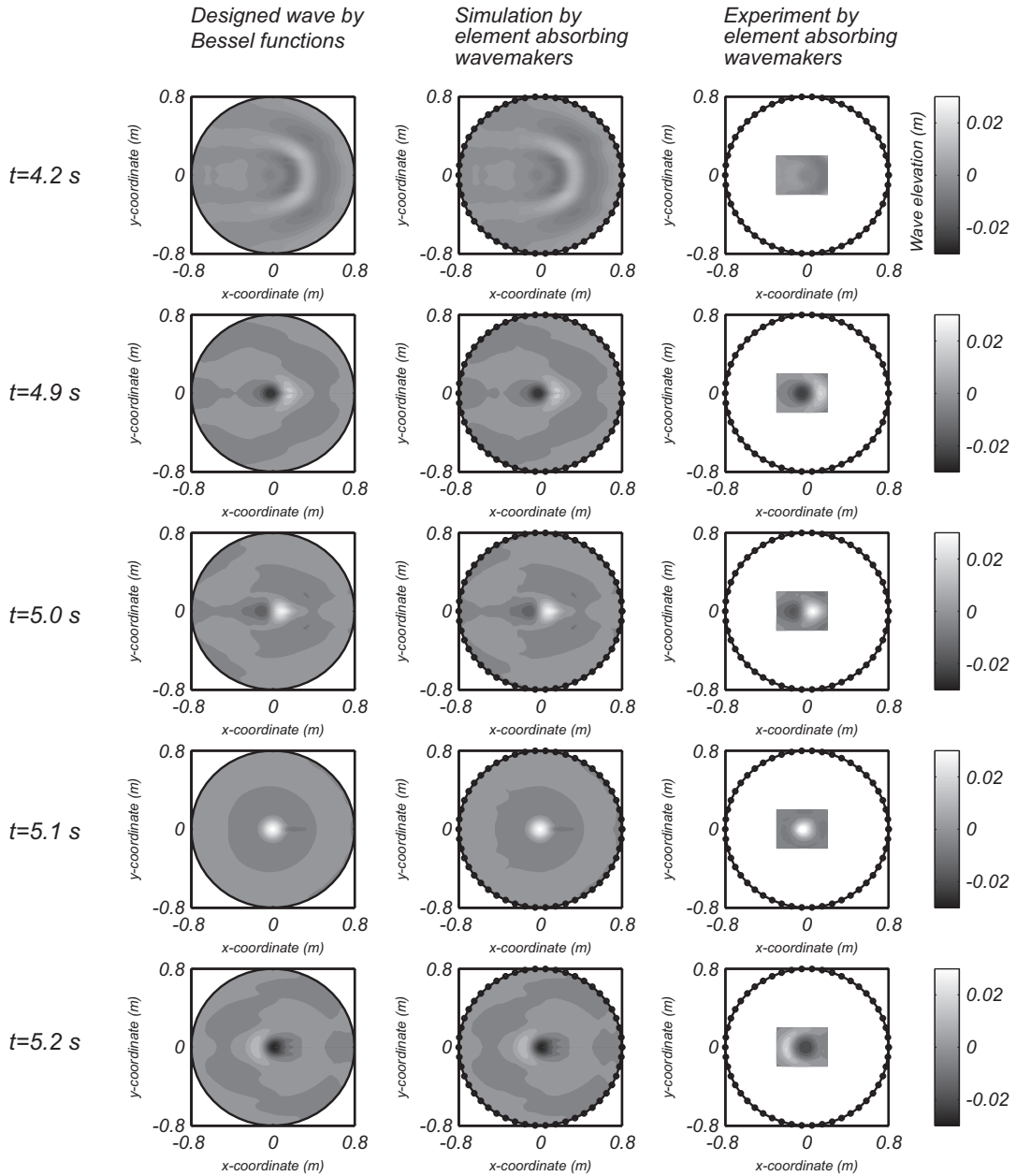
Designed wave by Bessel functions   *Simulation by element absorbing wavemakers*   *Experiment by element absorbing wavemakers*

Fig. 11 Wave contours before and after the designed extreme wave appears at t=5 s. Black dots put on the basin boundary express element absorbing wave-makers.

The complex wave elevation of the extreme wave is described by the Fourier series expansion:

$$\hat{\zeta}_a(r,\theta) = \sum_{\mu=-M}^{M} \sum_{\nu=-\infty}^{\infty} D_\nu \exp\left\{-i\kappa_\nu r \cos(\theta - \varphi_\mu)\right\}. \quad (30)$$

Substituting Eq. 30 into Eq. 18 or Eq. 21 gives C_{nm}. The wave generation force of element wave-makers is obtained by Eq. 13.

GENERATION OF EXTREME WAVE

Although the configuration of the *AMOEBA* can be changed for the aim of experiments, it was used as the circular basin with a radius of 0.8m and a depth of 0.25m. The Dini expansion was applied for the determination of wave generating forces of element absorbing wave-makers. C_{nm} was obtained by Eq. 18, when $p_n = 1$ was adopted. The transfer function $F(\omega)$ of the element absorbing wave-maker has been obtained by Naito *et al.*(1999, 2006). The wave elevation of the extreme wave was measured with a capacitance-type wave height gauge at 2cm mesh interval in a rectangle area of $x = -0.3$m to 0.2m and $y = -0.2$m to 0.2m
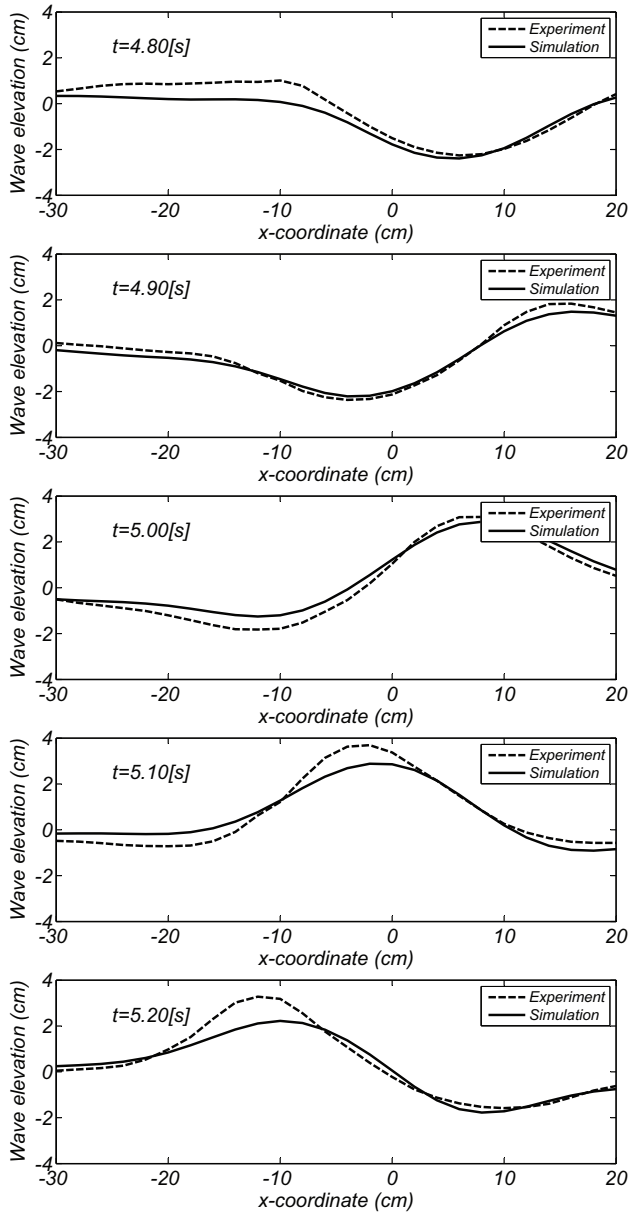
Fig. 12 Wave elevation on the x-coordinate at $t = 4.8$ to 5.2s.

Fig. 13 Time series of wave elevation at five points on the x-coordinate.

as shown in Fig. 10. The number of wave-height gauge points are 546.

Fig. 11 shows the wave contours of the design wave, the simulated wave and the experimental wave before and after the appearance of the extreme wave. The designed wave by the Bessel functions described in the left-hand section of Fig. 11 is obtained from Eq. 17 and the simulated wave by element absorbing wavemakers described in the center section of Fig. 11 is obtained from Eq. 18. Waves progress to the negative direction of the x-coordinate and gradually focus in the center of the basin. The extreme wave appear at the time $t = 5$s. Although the focused wave field expressed as an axial symmetrical contour appears at $t = 5.1$s, it is not the designed extreme wave. The simulated
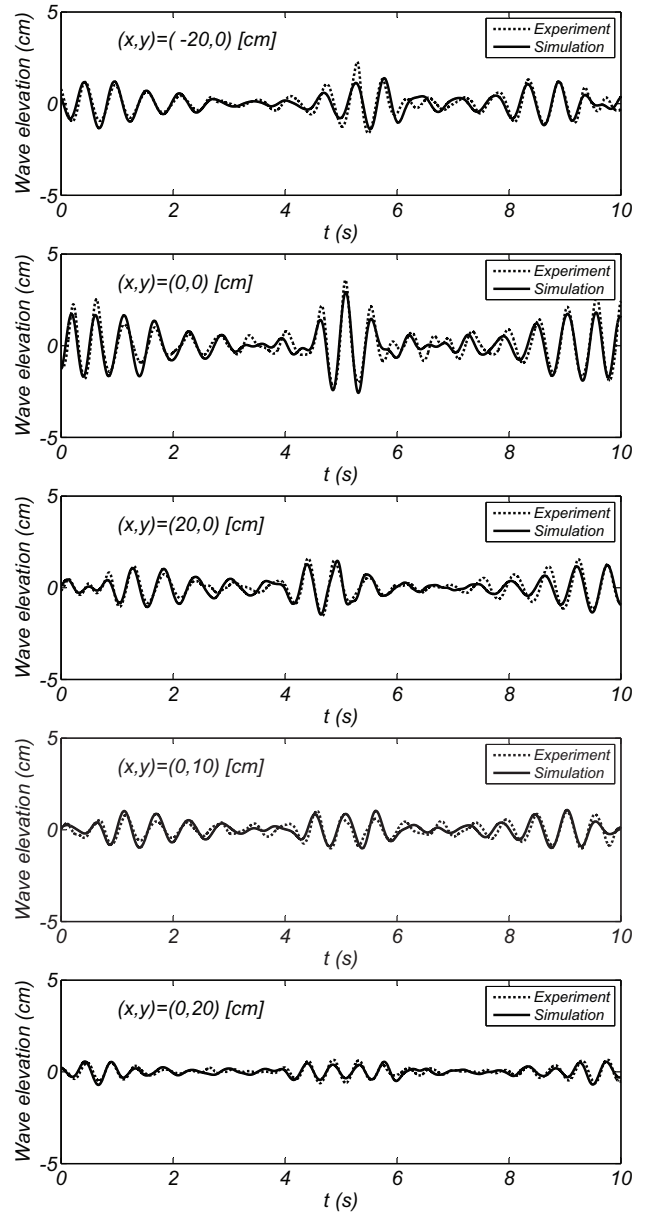
waves agree with the designed waves. These results convince of the correctness of the relation between Eq. 17 and Eq. 18. The simulated waves also express the experimental waves well.

To compare the profiles between simulated and experimental waves, we show the wave elevation appearing on the x-coordinate at $t = 4.8$s to 5.2s in Fig. 12. The experimental wave has almost same profile as the simulated wave at $t = 4.9$s and 5.0s. The remarkable difference appears at $t = 5.1$s and 5.2s. Then the experimental wave has a sharper crest and flatter trough than the simulated wave. The crest of the experimental wave is located forward of the crest of the simulated wave. This is caused by water depth and the nonlinearity due to wave steepness.

Fig. 13 shows the time series of wave elevation at five points on

the x-coordinate. In each point both wave elevations are almost same except crests and troughs as well as Fig. 12.

From Fig. 12, the gradient of wave surface at $x = 0$ and $t = 5.0$s is obtained as

$$\left.\frac{d\zeta(x,t)}{dx}\right|_{x=0,t=5} = \begin{cases} 0.473 & \text{for experimental wave,} \\ 0.327 & \text{for simulated wave.} \end{cases}$$

The wave steepness of gravity wave is limited to $1/7$ and then the maximum of the gradient of wave surface is $\pi/7 = 0.449$. The limit of the gradient of wave surface appears in the extreme wave obtained by experiments. Although we cannot discuss the accuracy of wave height and steepness because the simulated wave is approximately calculated by superposing ring waves based on the linear theory, the generation of the extreme wave designed arbitrarily is possible by using the proposed method.

CONCLUSIONS

A ring wave generated by an element absorbing wave-maker put on the circumference of the circular basin (*AMOEBA*) can be described by the Hankel function of the first kind in the linear theory. According to the addition theorem of the Hankel function, the superposition of this wave mathematically provides the n-th order Bessel function of the first kind with the origin in the center of the basin. Because an arbitrary wave field is decomposed into the Bessel functions and each Bessel function is decomposed into the Hankel function, an arbitrary wave field generated in a circular wave basin, of which basin wall is filled with element absorbing wave-makers, can be represented by superposing of ring waves expressed by the Hankel function. The wave generating force of an element absorbing wave-maker is obtained by applying the transfer function for the amplitude of the Hankel function.

The extreme wave is a focused wave with big height and steepness appearing at a specific point. This wave is also an arbitrary wave. Although it radically has nonlinear characteristics, it can be approximately decomposed into ring waves described by the Hankel function by means of the Fourier-Bessel series expansion and the Dini expansion. The extreme waves by simulation agrees well with the extreme wave by experiment in the *AMOEBA*. As the result, the proposed method of generating the extreme waves is clarified to be useful.

The detail of the wave profile by experiment is exactly different from that by simulation. It is casued by the nonlinearity of wave and the fact that a ring wave generated by a real element absorbing wave-maker is approximated by a wave source point. The weakly nonlinearity is expressed by the second order solution. However, it is difficult to generate and control the second order wave by the element absorbing wave-maker of the *AMOEBA*, taking account into the permitted frequency range of the current wave-maker. The future works would be focused on generating and evaluating anothor extreme wave.

REFERENCES

Madsen, O. S. (1974), A Three-Dimensional Wave-maker, Its Theory and Application, *Journal of Hydraulic Research*, Vol. 12, No. 2, pp. 205-222.

Ishida, S. and Watanabe, I. (1984). Properties of oblique waves generated by snake motion of segmented wave-maker, *Transactions of West-Japan Society of Naval Architects*, No. 67, pp. 135 (in Japanese).

Takezawa, S. and Hirayama, T. (1992). New Experimental Techniques on Ship Motions in Directional Spectrum Waves, *Proc. of 19th ONR Symposium* (*by Office of Naval Research*).

Naito, S. and Minoura, M. (1999). Evaluation of Performance of New Wave Making Basin, *Proc. of 9th International Offshore and Polar Engineering Conference*, Vol. 3, pp. 396-403.

Naito, S. and Minoura, M. (1994). Research on Element wave-makers and Wave Field Generated by Their Combination, *Proc. of 4th International Offshore and Polar Engineering Conference*, Vol. 3, pp. 8-16.

Naito, S., Minoura, M., Sakashita, H. and Tanaka, K. (1998). A New Concept of Wave Making Basin", *Proc. of International Workshop on Modeling of Ocean Environments in Wave and Current Basin (RealSea '98)*, pp. 95-112.

Naito, S. (2006). Wave Generation and Absorption -Theory and Application-, *International Journal of Offshore and Polar Engineering*, Vol. 16, No 2, pp. 81-89.

Milgram, I. H. (1970). Active Water Wave Absorbers", *Journal of Fluid Mechanics*, Vol. 43(4), pp. 845.

Falnes, J. and Budal, K. (1978). Wave-Power Conversion by Point Absorber", *Norwegian Maritime Research*, Vol. 6, No. 4.

Bessho, M. and Yamamoto, 0. (1980). Characteristics of New Wave-Energy Conversion Devices, *Proc. of 13th ONR Symposium (by Office of Naval Research)*, pp 841.

Salter, S. H. (1981). absorbing wave-makers and wide tanks, *Proc. of Directional Wave Spectra Applications, Berkeley, Am. Soc. Civ. Eng.*, pp. 185-202.

Abramowitz, M. and Stegun, I. A. (1972). Handbook of Mathematical Functions, *Dover Publications Inc.*.